Available online at www.sciencedirect.com
ScienceDirect
Journal of Solid State Chemistry 179 (2006) 3798–3804
JOURNAL OF SOLID STATE CHEMISTRY
www.elsevier.com/locate/jssc

Energetics of charge order transition in $Bi_{1-x}Sr_xMnO_3$

D. Sedmidubský[a,*], A. Strejc[a], O. Beneš[a], K. Ružička[a], J. Hejtmánek[b], P. Javorský[c], M. Nevřiva[a], C. Martin[d]

[a]*Institute of Chemical Technology, Technická 5, 166 28 Prague 6, Czech Republic*
[b]*Institute of Physics of ASCR, Cukrovarnická 10, 162 53 Prague 6, Czech Republic*
[c]*Faculty of Mathematics and Physics, Charles University, Ke Karlovu 3, 121 16 Prague 6, Czech Republic*
[d]*Laboratoire CRISMAT, 6 Boulevard Maréchal Juin, 14050 Caen Cedex, France*

Received 28 February 2006; received in revised form 21 August 2006; accepted 21 August 2006
Available online 24 August 2006

Abstract

The transition from the high-temperature pseudocubic form of the perovskite manganites $Bi_{1-x}Sr_xMnO_3$, $x = 0.3, 0.5, 0.8$, to their orthorhombically distorted charge-ordered state is examined. As the experimental probe the measuring of the heat capacity by heat flux DSC incremental method above 300 K and by relaxation method below 300 K is used. While a broad symmetrical transition spanning the temperature interval $\Delta T \sim 500$ K with a maximum at the apparent $T_{CO} \sim 500$ K is observed for $x = 0.5$, the other two compositions reveal typical λ-shaped peaks often considered as typical for the second order transitions. The total entropy release on heating is interpreted in terms of a simultaneous change of charge, orbital and spin degree of freedom.

PACS: 75.47.Lx; 71.30.+h

Keywords: Manganites; Charge order; Heat capacity

1. Introduction

The charge ordering (CO) transition in bismuth-based manganites, in $Bi_{1-x}Sr_xMnO_3$ system in particular, belongs to the most intriguing phenomena which have been recently discovered [1]. The CO-state leading to a localization of Mn-e_g electrons is established as a result of a strong electron–phonon interaction especially for integral ratios Mn^{3+}/Mn^{4+} ($x = \frac{1}{2}, \frac{1}{3}$, etc.), where a great portion of elastic energy is released due to simultaneous development of cooperative Jahn–Teller distortions of -($Mn^{3+}O_6$)-octahedra. The latter effect, that is inherently linked to CO, is often referred to as orbital ordering (OO). However, compared to other manganite systems with a general formula $Ln_{1-x}A_xMnO_3$ (Ln = lanthanide and A = alkaline earth) the CO transition occurs in $Bi_{1-x}Sr_xMnO_3$ at exceptionally high temperatures and, moreover, the maximum $T_{CO} \sim 610$ K is not achieved for the usual commensurate ratio $x = \frac{1}{2}, \frac{1}{3}$ or $\frac{2}{3}$, but for the composition with the highest Bi-content ($x \sim 0.25$) achievable using standard synthesis conditions [2]. This fact points to a peculiar role of bismuth ion whose stereoactivity manifested by an easy polarization of the $Bi^{3+} - 6s^2$ lone pair (hybridized with $-6p$ orbitals) gives presumably rise to the softening of the corresponding phonon modes and to a subsequent cooperative lattice distortion.

The half-doped $Bi_{0.5}Sr_{0.5}MnO_3$ is undoubtedly the most widely explored composition in the series. The different slope of inverse susceptibility below and above CO transition suggests a formation of Zener pairs (ZP) [3] with an overall spin $S = \frac{7}{2}$ which start to develop below $T_{CO} \sim 530$ K. The long-range antiferromagnetic order sets in at significantly lower temperature below $T_N \sim 150$ K [4]. A pertinent spin arrangement has been proposed as a superposition of two CE-type lattices with spins along x and y directions [4]. The simple ZP scenario assuming a delocalized e_g electron between two adjacent Mn atoms is,

*Corresponding author. Fax: +420 2 311 2206.
E-mail address: sedmidub@vscht.cz (D. Sedmidubský).

0022-4596/$ - see front matter © 2006 Elsevier Inc. All rights reserved.
doi:10.1016/j.jssc.2006.08.021

however, in apparent contradiction with the HREM images that clearly show a double-stripe type of modulation [5]. In order to bring the above two findings in accordance one has to consider, within a given Mn–Mn pair, a charge separation accompanied by a strong double exchange spin correlation. It should be also noted that CO/OO develops gradually below the apparent T_{CO} characterized by a metal–insulator (MI) transition and an onset of orthorhombic distortion down to ~300 K, which corroborates with the observed evolution of the modulation vector oriented along *a*-direction from $\mathbf{q} = 0.38$, determined at 500 K to $\mathbf{q} = 0.5$ at 300 K [6].

The magnetic and structural properties of Bi-rich compositions ($x < 0.5$) have been studied by Frontera et al. [2,7–9]. For $x = 0.25$ (with 2 wt% impurities of Bi_2O_3 and Mn_3O_4) they found, similarly to $x = 0.5$, a change of effective magnetic moment from $\mu_{eff} = 4.68$ (above) to 5.26 (below) when crossing T_{CO}. This has been argued to be also concomitant with ZP formation [2] that should coexist with 40% of Mn^{3+} ions for the charge balance to be preserved [9]. The CO/OO phase has been found to have an *Ibmm* subcell symmetry and a superstructure doubling the *a* and *c* lattice parameters. The magnetic order established below $T_N = 120$ K has been reported as antiferromagnetic (pseudo-CE type) although a significant net ferromagnetic component has been indicated in low fields [7,8].

The Sr-rich compositions exhibit a nearly linear decrease of the MI transition temperature with increasing Sr content as has been shown for $x = 0.5$–1.0 on resistivity and thermopower measurements [10]. For $x = 0.8$ composition both the MI transition and the onset of orthorhombic distortion occur simultaneously just below the ambient temperature (~280 K). Since in this case the Bi^{3+} ions are fairly diluted within the large cation sublattice, one can expect a similar behavior that is encountered in analogous manganite systems such as $Pr_{1-x}Sr_xMnO_3$. Let us remember that for $x > 0.6$ the $Pr_{1-x}Sr_xMnO_3$ structure adopts an OO-induced distortion characterized by d_{z^2} orbital polarization (without any apparent CO) followed by a C-type AF ordering.

In view of the present state of knowledge of CO/OO (CO and/or OO) phenomena in bismuth-based manganite perovskites it would be challenging to evaluate and analyze the energetic aspects of the above-mentioned transitions. The heat capacity has been measured recently by Gupta et al. [11] from 350 K up to above T_{CO} using a modulated DSC for $Bi_{1-x}Sr_xMnO_3$ compositions ranging from $x = 0.25$ to 0.75, and the temperature evolution of T_{CO} (indicated as a peak maximum) with x has been well reproduced. However, due to a poor quality of these C_p data, no quantitative information such as energy and entropy of the transition and the general thermodynamic functions can be recovered.

In this paper, we thus present the results of more accurate heat capacity measurements performed using three different techniques in a broad temperature range from 2 K up to well above the transition temperature T_{CO} for three selected samples from the $Bi_{1-x}Sr_xMnO_3$ series. Based on a thorough analysis of the phonon part of the C_p for a generic perovskite lattice we are able to extract the remaining excess component associated with the spin and charge/orbital ordering and to examine the temperature evolution of the corresponding enthalpy and entropy change.

2. Experimental

The samples were synthesized by conventional solid state reaction from binary oxides or carbonates (Bi_2O_3, $MnCO_3$—99.9%, Aldrich, $SrCO_3$—99.5%, Fluka). All chemicals were analyzed, respectively, for Bi, Mn and Sr prior to further processing. Appropriate amounts of starting components were mixed and homogenized and the resulting mixtures were repeatedly heated at 900 and 1000 °C in air. The calcined powders were compacted into pellets by uniaxial pressing under p~500 MPa and subjected to final heat treatment for 50 h. The samples with $x = 0.3$ and 0.5 were treated at 1050 °C in air, whereas the $x = 0.8$ sample was sintered at $T = 1180$ °C in argon atmosphere. The different treatment of the latter sample was applied in order to avoid stabilization of the hexagonal α-$SrMnO_3$ phase at the expense of the perovskite solid solution that occurs for Sr-rich compositions in normal air atmosphere. The resulting oxygen deficient perovskite structure was subsequently oxidized by a non-equilibrium annealing at 400 °C in O_2 gas. The final oxygen stoichiometry was checked by chemical analysis. The phase purity of the synthesized samples was probed by X-ray powder diffraction performed on Bruker D8 apparatus using Cu K_α radiation (40 kV, 30 mA) in the range 15–80° 2Θ (scanning step 0.02°).

The PPMS facility (Quantum Design) was used for the heat capacity measurements in the temperature range of 2–320 K. It is a fully automated equipment using a hybrid adiabatic relaxation technique. The PPMS software employs a two-tau relaxation method to evaluate the C_p values. Prior to each run with a given sample a blank run was performed to determine the addenda associated with the sample holder and Apiezon grease. The accuracy of these heat capacity measurements is estimated to ~1%.

The SETARAM high-temperature calorimeter (Multi HTC 96) with a mounted heat flux DSC detector was used for the heat capacity determination in the temperature range of 340–820 K (860 K for $x = 0.5$). The measurements were carried out in the incremental temperature scanning mode with a number of 10 K steps (heating rate 1.0 K min^{-1}) followed by isothermal delays of 5500 s. Three runs were performed to obtain the C_p of each sample—one with an empty crucible (blank), the second one with the reference material (synthetic sapphire, NIST Standard reference material No. 720) and the third one with a given sample. All measured and reference samples were used in powdered form. The typical sample mass was 1 g. The

accuracy of heat capacity measurements is estimated to be better than 4% with this technique.

In order to get more accurate results around the CO-transition and a larger overlap with low-C_p data for the $x = 0.5$ sample, we employed Calvet-type Setaram C-80 calorimeter operated also in an incremental scanning regime and in the temperature interval 300–600 K. In this case the used heating rate was slower (0.2 K min^{-1}), while the delay intervals were prolonged to 9000 s. The temperature increments varied from 5 to 10 K depending on temperature. With typical sample masses 13–16 g the achieved accuracy is ~2%.

3. Results and discussion

The measured heat capacities of the investigated samples are plotted in Fig. 1. In all three cases the high-temperature DSC data, although more scattered, join smoothly the low-temperature PPMS curves. The CO/OO transition is manifested by pronounced peaks on C_p curves with the maxima corresponding to the ordering temperatures T_{CO} which reveal a descending trend with increasing x. Let us note that the transition temperature is denoted, for the sake of simplicity, as T_{CO} even for $x = 0.8$ sample where no definite charge ordering is anticipated. The particular values given in Table 2 are consistent with the characteristic temperatures identified from electric transport data as metal–insulator-like transition [10], the onset of the structural distortion (the average structure below T_{CO} was indexed using *Imma* space group) and the threshold of the change of magnetic state indicated on the temperature evolution of *DC*-magnetic susceptibility [2,4].

In order to examine the CO/OO transition itself it would be desirable to separate the excitations corresponding to the disruption of magnetic and charge/orbital order from the lattice part of the heat capacity pertinent to a generic (though idealized) perovskite manganite exhibiting no such transitions. Since all three compositions reveal an insulator ground state, no electronic specific heat is anticipated at low temperatures. Disregarding the symmetry lowering due to OO effects observed in many manganites, the ideal cubic perovskite unit cell contains five atoms and its phonon spectrum can thus be reasonably approximated by 15 normal vibration modes. Accordingly, the respective lattice heat capacity in harmonic crystal approximation can be written in terms of three degenerate Debye modes representing the acoustic branches and four triply degenerate Einstein modes that substitute the remaining 12 optical phonon bands. This hybrid Debye–Einstein (D–E) model can be expressed as

$$C_{\mathrm{lat}} = 9\mathbf{R}\left(\frac{T}{\Theta_{\mathrm{D}}}\right)^3 \int_0^{\Theta_{\mathrm{D}}/T} \frac{x^4 \mathrm{e}^x}{(\mathrm{e}^x - 1)^2}\,\mathrm{d}x + 3\mathbf{R}\sum_I \frac{(\Theta_{\mathrm{EI}}/T)^2 \mathrm{e}^{\Theta_{\mathrm{EI}}/T}}{(\mathrm{e}^{\Theta_{\mathrm{EI}}/T} - 1)^2} + C_{\mathrm{an}}. \quad (1)$$

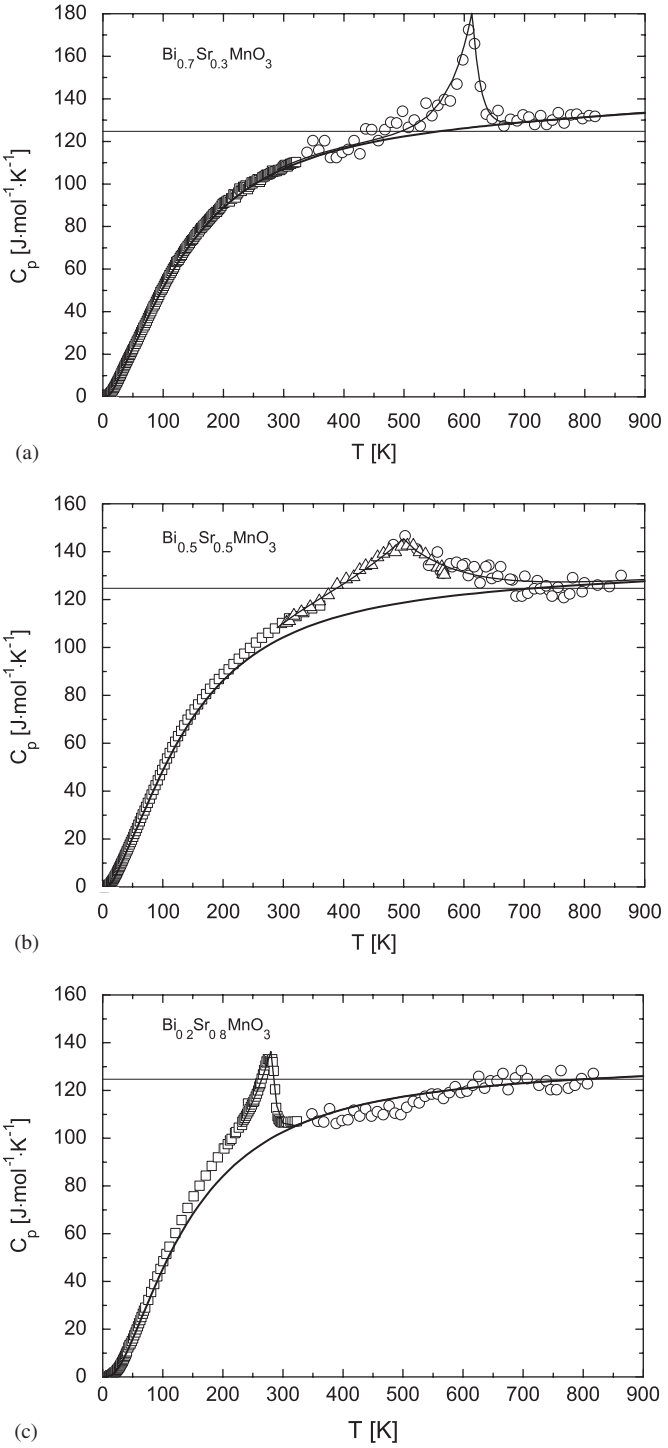

Fig. 1. Measured heat capacities vs. temperature. (a), (b), (c) for $x = 0.3, 0.5, 0.8$, respectively. □—PPMS data, ○—DSC data (Multi HTC 96), △—DSC data (C-80). Horizontal line—Dulong–Petit limit, full-line curves—Debye–Einstein fit and CO/OO transition approximated by Eq. (2).

Here each mode is represented by a characteristic temperature Θ_{D} and Θ_{EI}, where I in Einstein modes stands for T, B, S, and L denoting, respectively, tilting, bending and stretching modes of -[MnO_6]-octahedra and vibration modes of large cation. Furthermore, to take into account

anharmonic effects which are responsible for the roughly linear (in T) $(C_p - C_V)$ term in lattice heat capacity, we use the well known phenomenological formula $C_{an} = (C_p - C_V) = TV_m\alpha^2/\beta$, where α stands for the isobaric volume expansion coefficient and β for the coefficient of the isothermal compressibility.

The parameters of the D–E model (Eq. (1)) have been recently evaluated for 15 different manganites and correlated with the occupation of the large cation site [12]. While the Debye and large cation modes revealed roughly linear dependencies $\Theta_D = 489 - 1.27\ M_p$ and $\Theta_{EL} = 281 - 0.482\ M_L$ on the molar masses of the whole compound M_p and the large cation M_L, the characteristic temperatures of the tilting, bending and stretching modes were not found to show any apparent trend. They attain the average values $\Theta_{ET} = 398 \pm 54$, $\Theta_{EB} = 514 \pm 28$ K, and $\Theta_{ES} = 767 \pm 13$ K. The volume expansion coefficient treated as a fitting parameter was found $\alpha = (4.4 \pm 0.8 \times 10^{-5}\,K^{-1}$, whereas a constant isothermal compressibility assuming a typical value for transition metal perovskites $\beta = 7 \pm 3 \times 10^{-3}\,GPa^{-1}$ [13] was considered in all cases. The parameter values resulting from this analysis were used as an initial guess and modified within the respective error bars (except for Θ_{ES} for which higher values had to be considered) to get a least-square fit of those parts of the experimental C_p data where no effects related to CO/OO and magnetic transitions were expected.

The optimized values are compiled in Table 1 and the resulting calculated curves of C_{lat} are plotted in Fig. 1 together with the experimental data. For a comparison, the results from an analogous analysis performed on the cubic perovskite β-$SrMnO_3$ [12] are also given in Table 1. Due to lower values of Θ_D the Bi-rich composition exhibits a more rapid saturation of the harmonic part of C_{lat} towards the Dulong–Petit limit (15**R**) and as a result of higher α it also crosses the 15**R**-line at lower temperature. This is in accordance with larger mass of Bi (lower Θ_D) and its higher polarisability implying softer phonon modes and higher anharmonic contribution C_{an}. The characteristic temperatures of Einstein modes show, with the exception of Θ_S, only a weak variation with x. Θ_S is appreciably lower for $x = 1.0$ compared to Bi-containing compositions, which might be linked to higher stiffness of the stretching modes related to Jahn–Teller distorted Mn^{3+} octahedra. The fitted values of α are, within the indicated error bars, in agreement with those evaluated from lattice parameter evolution [4,8] and those reported for other transition metal perovskites [13].

In addition to the D–E model the C_{lat} part was expressed in terms of a polynomial fit valid above 298 K, which is a conventional form of presentation of C_p data in thermochemical tables (see Table 2). Based on the D–E analysis outlined above we were able to separate the excess part C_{exc} inherent to CO/OO and magnetic ordering effects by subtracting the calculated C_{lat} (Eq. (1)) from the measured data. The resulting peaks were then fitted using a formula proposed for magnetic transitions in metals [14]

$$C_{CO} = k(T/T_{CO})e^{q(1-T/T_{CO})} \quad (2)$$

treating separately the parts above and below the CO/OO transition. The analysis results are summarized in Table 3.

Although Eq. (2) was adequate to describe the excess part in the high-temperature region attributable to CO/OO, all three compositions show additional features at lower temperatures, which are evidently caused by magnetic ordering. For $x = 0.5$ and 0.8 this anomaly has a form of low-temperature shoulder of the C_{exc} peak, while for $x = 0.3$ it is well separated from the CO/OO effect. Due to parabolic-like shape it was not possible to use Eq. (2) for the peak description and the relevant data were only splined. Shown in Fig. 2 are both the magnetic and CO/OO peaks, as well as the overall C_{exc} curve. The magnetic peak maximum at ~140 K fairly corresponds to $T_N = 150$ K found by *DC*-susceptibility measurements in the half-doped sample [4]. For the $x = 0.8$ composition the high-temperature onset of the magnetic peak at ~210 K can be identified with a cusp seen on *DC*-susceptibility curve [15] suggesting presumably an onset of antiferromagnetic ordering. In the $x = 0.3$ case the low-temperature effect extends markedly above $T_N = 120$ K reported as a Néel temperature for pseudo-CE antiferromagnetic structure [8]. In summary, the magnetic ordering can be detected on the C_{exc} curve, though it is a rather indistinctive feature in comparison with some other manganites such as $LaMnO_3$ or $CaMnO_3$.

As mentioned, the CO/OO transition in $x = 0.5$ is accompanied by a gradual decrease of the modulation vector over a temperature interval from ~375 K up to T_{CO} (see Fig. 3, [6]). The lower temperature corresponding to a saturation towards $\mathbf{q} = 0.5$ coincides with an abrupt

Table 1
Characteristic temperatures of the Debye (Θ_D) and Einstein (Θ_{EL}, Θ_{ET}, Θ_{EB}, Θ_{ES}) vibration modes for a generic perovskite lattice (Eq. (1)) and the volume expansion coefficient α evaluated from the measured heat capacities

x	Θ_D	Θ_{EL}	Θ_{ET}	Θ_{EB}	Θ_{ES}	α
	(K)					($10^{-5}\,K^{-1}$)
0.3	140 ± 3	255 ± 25	410 ± 46	500 ± 61	850 ± 35	5.0 ± 0.6
0.5	155 ± 2	270 ± 3	420 ± 13	510 ± 41	875 ± 34	3.5 ± 0.7
0.8	205 ± 13	280 ± 35	430 ± 56	520 ± 53	900 ± 45	3.0 ± 0.6
1.0	234 ± 12	254 ± 22	424 ± 65	550 ± 56	764 ± 41	3.5 ± 0.7

Table 2
Parameters obtained from the heat capacity analysis—coefficients of the lattice part polynomial fit $C_p = a + b \cdot T + c/T^2$, $T \geqslant 298$ K

x	a	b	c
	($J\,mol^{-1}\,K^{-1}$)		
0.3	120.0 ± 0.7	$(1.742 \pm 0.089) \times 10^{-2}$	$(1.620 \pm 0.044) \times 10^{6}$
0.5	119.5 ± 0.8	$(1.172 \pm 0.096) \times 10^{-2}$	$(1.679 \pm 0.048) \times 10^{6}$
0.8	119.0 ± 0.8	$(1.063 \pm 0.103) \times 10^{-2}$	$(1.749 \pm 0.051) \times 10^{6}$

Table 3
Coefficients T_{CO}, k, q of the excess part exponential fit (Eq. (2)). Subscripts l and u denote, respectively, the part below and above T_{CO}

x	k_l	k_u	q_l	q_u	T_{CO}
	($J\,mol^{-1}\,K^{-1}$)		(K^{-1})		(K)
0.3	53.8 ± 1.8	58.1 ± 1.5	14.9 ± 0.9	47.3 ± 2.7	612 ± 1
0.5	27.1 ± 0.6	25.2 ± 1.6	2.6 ± 0.1	5.9 ± 0.5	502 ± 1
0.8	35.7 ± 0.4	45.9 ± 2.6	4.3 ± 0.2	34.5 ± 2.5	279 ± 1

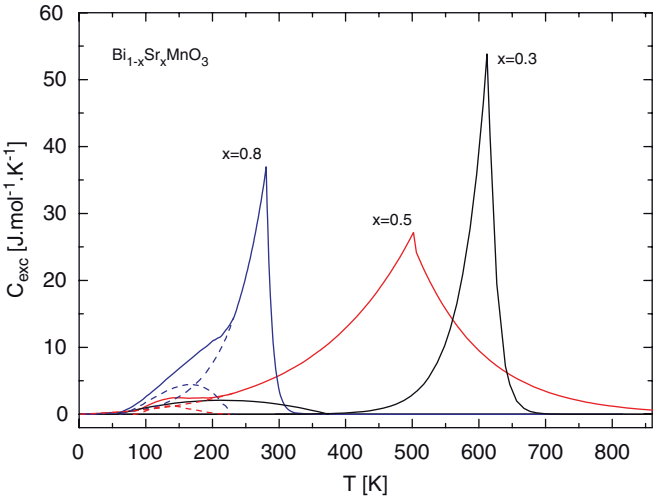

Fig. 2. Excess part of the heat capacity corresponding to CO/OO and magnetic transition. The dashed lines in $x = 0.5$ and 0.8 represent the separate CO/OO and magnetic contributions. The CO/OO part was fitted using Eq. (2).

change of slope on the temperature dependence of lattice parameters reported in [4]. Moreover, the extrapolation of the observed linear dependence of **q** slightly above T_{CO} towards the temperature of disappearance of the orthorhombic distortion, $T \sim 540$ [4], yields another commensurate value of $\mathbf{q} \sim \frac{1}{3}$. Hence, we are dealing rather with a broad crossover supposedly driven by a gradual softening of the corresponding phonon modes (with gradually evolving wave vector) ending up at 375 K in a complete development of a commensurate superstructure with a doubled unit cell. The local structural distortions on Mn-sites accompanying this process invoke simultaneously the orbital polarization and the partial charge separation. Our

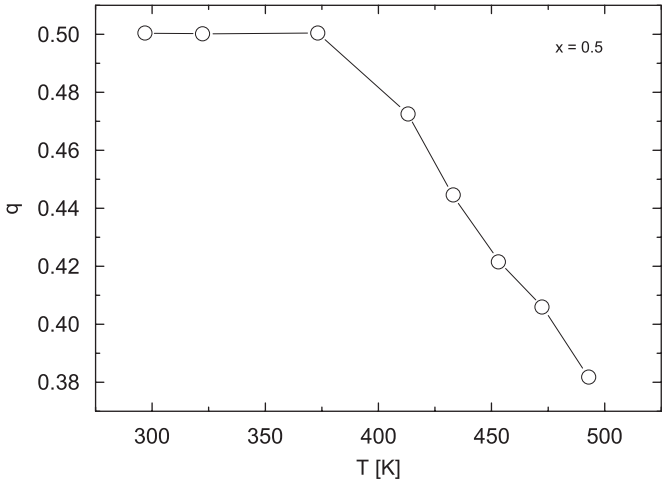

Fig. 3. Temperature dependence of the norm of modulation vector **q** coincident with its q_a component as observed by electron diffraction on the $x = 0.5$ sample. Adopted from Ref. [6].

heat capacity data which show a broad peak on C_{exc} spanning from ~250 K up to ~800 K (Fig. 2) seem to be in agreement with this scenario. Note that this picture contradicts the simple ionic model based on an ordering of point charges identified with Mn^{3+} and Mn^{4+}. However, in addition to this gradual development of charge ordered phase, one should also consider a possible phase separation (CO vs. charge disordered phase) in the intermediate temperature range as recently documented on atomically resolved STM images [11].

Interestingly, the CO/OO transition is much narrower (~200 K) for ratios $x = 0.3$ and 0.8. In the former case, the peak width can be again correlated with the evolution of orthorhombic distortion reported in Refs. [8,9]. The onset at ~600 K of the transition from *Pbnm* to *Ibmm* symmetry accompanying CO/OO [9] lies only 12 K below our peak maximum and the saturation of the distortion observed at ~520 K is also in fair agreement with the down-set of the C_{exc} peak tail. Unfortunately, no such structural data are available for $x = 0.8$. Nevertheless, the transitions in both cases are manifested by typical λ-shaped peaks with only weak correlations persisting above T_{CO} and a rapidly developing ordering parameter saturating ~100 K below T_{CO}. In a clear contrast to that, the $x = 0.5$ sample exhibits a nearly symmetrical peak that extends ~300 K both below and above T_{CO}. This might seem as a surprising result when considering merely the Mn-sublattice. In such a case one would expect the largest driving force to CO/OO resulting in an abrupt increase of the ordering parameter for the commensurate ratio $Mn^{3+}/Mn^{4+} = 1$. However, as stated above, in Bi-based manganites the Bi^{3+} lone pair and, consequently, the Bi concentration plays an indispensable role in the observed ordering transition by favoring the localization of e_g electrons and driving the structure in the CO/OO state. Indeed, the ordered phase with a composition very close to $x = 0.3$ has been found, in addition to the highest T_{CO} ever achieved, particularly

stable and homogeneous [9]. This brings us to a presumption that upon cooling even the $x = 0.5$ system is first driven to an ordering pattern characteristic for a ground state of Bi-rich composition and then, at lower temperatures, it gradually transforms to a superstructure specific for a half-doped system.

The relative enthalpies and standard entropies at a reference temperature of 298 K given in Table 4 were evaluated by integrating the experimental C_p and C_p/T data. Considering only the lattice part, C_{lat}, they should decrease with increasing Sr-content, but the OO transition taking place just below the reference temperature for $x = 0.8$ causes a turnover in the trend of relative enthalpy and a slowdown of entropy decrease.

The excess enthalpy and entropy, ΔH_{exc} and ΔS_{exc} (Table 4), calculated by integration of the excess part C_{exc} and C_{exc}/T reach their maximum for the half-doped composition, which should exhibit the highest mixing entropy on Mn-sublattice in the disordered state and also an ultimate enthalpy release is expected upon the development of the commensurate superlattice. It is difficult to draw quantitative conclusions regarding the enthalpy change, however, on the basis of a simple model considering separately the spin, orbital and Mn-sublattice occupation degrees of freedom we should be able to evaluate the overall entropy change associated with a transition from the disordered state to the completely ordered one (CO/OO/AFM). More specifically, taking into account the mixing entropy on Mn-site $-\mathbf{R}[x\ln(x) + (1-x)\ln(1-x)]$, spin entropy $\mathbf{R}[x\ln(4) + (1-x)\ln(5)]$ and the entropy linked to e_g-orbital degeneracy of Mn^{3+}, $\mathbf{R}(1-x)\ln(2)$ this scheme yields the values $\Delta S_{exc} = 21.94, 21.10,$ and $17.21\,J\,K^{-1}\,mol^{-1}$ for $x = 0.3, 0.5,$ and 0.8, respectively. These values are by 14.8, 7.1 and $4.6\,J\,K^{-1}\,mol^{-1}$ overestimated with respect to the experimentally determined data (Table 4).

In the case of $x = 0.3$, there is not yet a definite consensus on the magnetic ground state. Although an AFM-ordering of CE type has been reported in [7,8], a strong field induced FM component, the shape of the magnetization curve and a large apparent $\gamma \sim 40\,mJ\,K^{-2}\,mol^{-1}$ extracted from low-temperature C_p/T vs. T^2 dependence on our sample suggest a more complex magnetic state strongly reminiscent to spin/cluster glass formation. We may thus surmise that at least a part of the magnetic entropy is frozen in the $x = 0.3$ manganite. This should lead to lower ΔS_{exc} evaluated on a base of the measured C_p. The difference between the experimental and estimated values of ΔS_{exc} found for the other two samples can be ascribed to an incomplete ($x = 0.5$) or even absent ($x = 0.8$) charge separation in the ordered state, while the theoretical estimation is based on a purely ionic picture of complete ordering of Mn^{3+} and Mn^{4+} species. Nevertheless, an error caused by an inaccurate separation of C_{lat} and C_{exc} cannot be excluded, either.

Table 4
Enthalpies and entropies derived from the measured heat capacities

x	$H^\circ_{298} - H^\circ_0$ ($kJ\,mol^{-1}$)	S°_{298} ($J\,mol^{-1}\,K^{-1}$)	ΔH_{exc} ($kJ\,mol^{-1}$)	ΔS_{exc} ($J\,mol^{-1}\,K^{-1}$)
0.3	19.45	127.24	3.36	7.13
0.5	19.15	122.63	5.75	14.03
0.8	20.31	121.85	2.69	12.64

($H^\circ_{298} - H^\circ_0$)—relative enthalpy, S°_{298}—entropy at 298 K, ΔH_{exc}, ΔS_{exc}—excess enthalpy and entropy.

4. Conclusions

We have investigated the energetics of the order–disorder transition in the perovskite manganites $Bi_{1-x}Sr_xMnO_3$. The measurement of heat capacity of three selected compositions with variable Bi/Sr ratio on large cation sublattice revealed the occurrence of clear peaks, which can be unambiguously identified with the transitions to charge and/or orbital-ordered state. The apparent transition temperatures T_{CO} located at the corresponding peak maxima are identical or very close to values determined by complementary techniques. Whereas the half-doped sample reveals a broad and nearly symmetrical peak suggesting strong correlations well above T_{CO} and a slowly evolving superstructure below, both Bi- and Sr-rich compositions exhibit more conventional ordering behavior as indicated on the characteristic λ-shaped peaks. The Debye–Einstein analysis of the lattice part of C_p allowed to separate the C_{exc} attributed to CO/OO and magnetic ordering and to evaluate the pertinent enthalpies and entropies. The resulting entropies are lower compared to values estimated on the basis Mn^{3+}/Mn^{4+} ionic model considering spin, orbital and Mn-site occupation degrees of freedom. The largest discrepancy found for Bi-rich sample may be correlated with a broad featureless magnetic effect interpreted as a result of incomplete spin ordering and a consequent quenching of spin entropy.

Acknowledgments

Supported by the Czech Science Foundation, Grant No. 203/03/0924, and the Ministry of Education of CR, project No. MSM6046137302. A. Strejc greatly acknowledges the financial support of the EU Commission provided within the RTN SCOOTMO, project No. HPRN-CT-2002-00293.

References

[1] J.L. García-Muñoz, C. Frontera, M.A.G. Aranda, A. Llobet, C. Ritter, Phys. Rev. B 63 (2001) 064415.
[2] C. Frontera, J.L. García-Muñoz, C. Ritter, L. Manosa, X.G. Capdevila, A. Calleja, Solid State Commun. 125 (2003) 277.
[3] A. Daoud-Aladine, J. Rodríguez-Carvajal, L. Pinsard-Gaudart, M.T. Fernández-Díaz, A. Revcolevschi, Phys. Rev. Lett. 89 (2002) 097205.

[4] J. Hejtmánek, Z. Jirák, M. Hervieu, C. Martin, M. Nevřiva, P. Beran, J. Appl. Phys. 93 (2003) 7370.
[5] M. Hervieu, A. Maignan, C. Martin, N. Nguyen, B. Raveau, Chem. Mater. 13 (2001) 1356.
[6] P. Beran, Manganites à base de bismuth—Ètude du Système (Bi,Sr,Ca)MnO_3, Thesis, Université Caen-ICT Prague, 2004.
[7] C. Frontera, J.L. García-Muñoz, M.A.G. Aranda, M. Hervieu, C. Ritter, A. Calleja, X.G. Capdevila, M. Respaud, J. Appl. Phys. 97 (2005) 10C105.
[8] J.L. García-Muñoz, C. Frontera, M. Respaud, M. Giot, C. Ritter, X.G. Capdevila, Phys. Rev. B 72 (2005) 054432.
[9] C. Frontera, J.L. García-Muñoz, M.A.G. Aranda, M. Hervieu, C. Ritter, L. Ma nosa, X.G. Capdevila, A. Calleja, Phys. Rev. B 68 (2003) 134408.
[10] D. Sedmidubský, O. Beneš, P. Beran, J. Hejtmánek, M. Maryško, J. Magn. Magn. Mater. 272–276 (Suppl. 1) (2004) E285–E286.
[11] A. Gupta, S.B. Samanta, V.P.S. Awana, H. Kishan, A.M. Awasthi, S. Bhardwaj, A.V. Narlikar, C. Frontera, J.L. García-Muñoz, Physica B 370 (2005) 172.
[12] A. Strejc, Thermodynamic and structural properties of mixed valence oxides, Thesis, ICT Prague, 2005.
[13] S. Yamanaka, K. Kurosaki, T. Maekawa, T. Matsuda, S. Kobayashi, M. Uno, J. Nucl. Mater. 344 (2005) 61.
[14] Y.Y. Chuang, R. Schmid, Y.A. Chang, Metall. Trans. A 16A (1985) 153.
[15] O. Beneš, Charge ordering in Bi-based manganites, Thesis, ICT Prague, 2005.